Journal of Power Sources 196 (2011) 10038–10049

Contents lists available at ScienceDirect

Journal of Power Sources

journal homepage: www.elsevier.com/locate/jpowsour

Syngas suitability for solid oxide fuel cells applications produced via biomass steam gasification process: Experimental and modeling analysis

Elisa Pieratti[a], Marco Baratieri[b,*], Sergio Ceschini[c], Lorenzo Tognana[c], Paolo Baggio[a]

[a] University of Trento, Department of Civil and Environmental Engineering, Via Mesiano 77, 38123 Povo (TN), Italy
[b] Free University of Bolzano, Faculty of Science and Technology, Piazza Università 5, 39100 Bolzano, Italy
[c] Eurocoating S.p.a., via Al Dos De La Roda 60 – 38057 Cirè di Pergine (TN), Italy

ARTICLE INFO

Article history:
Received 19 April 2011
Received in revised form 17 July 2011
Accepted 23 July 2011
Available online 17 August 2011

Keywords:
Biomass
Steam gasification
Hydrogen sulphide
Equilibrium model
SOFCs

ABSTRACT

The technologies and the processes for the use of biomass as an energy source are not always environmental friendly. It is worth to develop approaches aimed at a more sustainable exploitation of biomass, avoiding whenever possible direct combustion and rather pursuing fuel upgrade paths, also considering direct conversion to electricity through fuel cells. In this context, it is of particular interest the development of the biomass gasification technology for synthesis gas (i.e., syngas) production, and the utilization of the obtained gas in fuel cells systems, in order to generate energy from renewable resources. Among the different kind of fuel cells, SOFCs (solid oxide fuel cells), which can be fed with different type of fuels, seem to be also suitable for this type of gaseous fuel. In this work, the syngas composition produced by means of a continuous biomass steam gasifier (fixed bed) has been characterized. The hydrogen concentration in the syngas is around 60%. The system is equipped with a catalytic filter for syngas purification and some preliminary tests coupling the system with a SOFCs stack are shown. The data on the syngas composition and temperature profile measured during the experimental activity have been used to calibrate a 2-dimensional thermodynamic equilibrium model.

1. Introduction

The gas produced through gasification process (i.e., syngas) can be used in several applications for separate or combined heat and power generation, and for the production of liquid fuels and chemicals. Several goals have been achieved in the last 20 years in this research field, but the process efficiency and the tar removal are still a problem for most of the applications.

The syngas produced can be used for power generation in a CHP cycle (combined cycle for heat and power generation). In these systems the gas yield can be exploited in alternative internal (IC) combustion engines. Modified gas engines can be fed with gas of different quality, even those having calorific values around 5 MJ Nm^{-3}. The output energy can be roughly divided up as one-third electric energy and two-third thermal energy.

IGCC (integrated gasification combined cycles) are preferred – instead of CHP systems based on alternative engines – for the electricity generation on larger scale. In these systems the synthesis gas is burned in the combustion chamber of a gas turbine. However, gas turbines requires a pressurized gas supply line, thus the syngas has to be compressed or directly produced in a pressurized gasification unit at a pressure of 5–20 bar. The major drawback for pressurized gasification is the cost related to the energy consumption to pressurize the gasifying agent and the inlet biomass.

Considering the existing experimental pilot plants, fuel cells can potentially achieve higher electrical efficiencies, compared with conventional internal combustion engines. A fuel cell installed downstream of a gasifier – after an enhanced cleanup stage – represents a coupled system (similar in size to an equivalent gasification – micro gas turbine generation system) characterized by high electric and overall efficiencies.

As confirmed by previous research studies available in the literature, the use of synthesis gas from biomass gasification in fuel cells is still in an early stage of application. The performance of integrated biomass gasifiers and SOFC systems has been investigated from a theoretical point of view by several authors [1–9].

Panopoulos et al. [2,3] studied the feasibility of high efficiency SOFC-CHP systems of sizes up to 1 MW_e with a novel allothermal steam gasification reactor. The reactor is heated by burning depleted SOFC off gas, un-reacted residual char and additional biomass if necessary. The STBR used is 0.6 to limit the heat required for the gasification system. The size of the system is based on 100 m^2 of SOFC active surface. The model results show a system electrical efficiency of 36% and a thermal efficiency of 14%.

* Corresponding author. Tel.: +39 0471 017201; fax: +39 0471 017009.
E-mail address: marco.baratieri@unibz.it (M. Baratieri).

0378-7753/$ – see front matter © 2011 Elsevier B.V. All rights reserved.
doi:10.1016/j.jpowsour.2011.07.090

Nomenclature

A	gasifier cross section area (m^2)
a	thermal diffusivity ($m^2\ s^{-1}$)
c_p	specific heat ($kJ\ kg^{-1}\ K^{-1}$)
H	specific enthalpy ($kJ\ kg^{-1}$)
ΔH	specific enthalpy variation ($kJ\ kg^{-1}$)
$\dot{m}$	mass flow rate ($kg\ s^{-1}$)
n	number of moles
$\boldsymbol{n}$	unit vector normal to the relevant surface
$\boldsymbol{N}$	Input vector in the thermodynamic model
p	pressure (Pa)
r	gasifier radial coordinate
$\dot{Q}$	heat source ($W\ m^{-3}$)
Q	thermal power (W)
T	temperature (K)
$\boldsymbol{u}$	velocity vector ($m\ s^{-1}$)
v	velocity component along the radial coordinate, r ($m\ s^{-1}$)
w	velocity component along the vertical coordinate, z ($m\ s^{-1}$)
W	average velocity on the gasifier cross section ($m\ s^{-1}$)
z	gasifier vertical coordinate
V	biomass volume (m^3)

Greek

η	efficiency
η_c	carbon conversion efficiency
ϕ	porosity
λ	thermal conductivity ($W\ m^{-1}\ K^{-1}$)
ρ	density ($kg\ m^{-3}$)
γ	adimensional parameter
ξ	biomass fraction converted into gas
τ	time constant (s)

Subscripts

0	values at the initial step (at the gasifier inlet)
A	air
B	biomass
C	carbon
E	heating condition on the external surface of the gasifier shell
G	syngas
H	hydrogen
O	oxygen
i	values at the *i*th step (in the gasifier)
IN	values at the gasifier inlet
OUT	values at the gasifier outlet
Q	flow ($NmL\ min^{-1}$)
R	reaction
S	steam condition on the internal coaxial tube of the gasifier
VAP	vaporization
W	water

Acronyms

CFD	computational fluid dynamic
LHV	lower heating value
PFD	process flow diagram
RT	room temperature
SC	steam to carbon: ratio between the moles of H_2O fed and the moles of carbon in the feedstock
STBR	steam to biomass ratio

Cordiner et al. [4] simulated a 14 kW energy generation system consisting of a SOFC stack fed by a biomass gasifier. The gasifier is integrated with a heat recovery system on the SOFC off-gas combustion, in order to enhance the energy performance. The gasifier has been simulated by means of a zero-dimensional equilibrium model, while a 3D CFD model has been implemented for the SOFC. The overall system efficiency has been assessed at 45%.

Omosun et al. [5] have developed a steady state model to investigate the performance of an integrated SOFC stack – biomass gasifier system. The model has been used to study the system efficiency and its costs considering two different options: "cold" gas cleaning at low temperature and "hot" gas cleaning at high temperature. The simulations show an overall system efficiency of 60% for the hot gas cleanup and 34% for the cold one.

Liu et al. [6] have assessed the theoretical performance of an integrated gasifier-SOFC pilot system which was under construction. It consists of a fixed bed gasifier and a 5 kW SOFC CHP system. Two solutions for gas cleaning have been considered: a combined low and high temperature gas cleaning system and a high temperature gas cleaning system. The results of the analysis show that the electrical efficiency of the CHP system considering the different gas cleaning units, are approximately the same, although the high temperature solution shows higher thermal efficiency both for the energy and exergy balance.

Nagel et al. [7–9] have researched on the technical and on the cost analysis of a biomass integrated gasification fuel cell (B-IGFC) system. The paper [9] shows some preliminary experimental results collected from a series of tests performed in the B-IGFC demonstration unit consisting of gasifier, gas cleaning session (with catalyst) and fuel cell stack. The gasifier and the catalytic unit could operate with a satisfying degree of reliability; the SOFC unit fed with syngas generates approximately 40% less current compared to methane operation. Ash deposition was the major obstacle for a smooth SOFC system operation.

The purpose of the present work is the evaluation of the feasibility of a B-IGFC for residential applications (i.e., micro-cogeneration system). The main interest is the analysis of the steam gasification process as a possible pathway to generate high quality syngas suitable for solid oxide fuel cells.

2. Modeling

2.1. Process conditions

The aim of the present work is a feasibility assessment of a B-IGFC micro-cogeneration system suitable for residential applications. The electric energy load required by 1–2 apartments has been considered for choosing the output of the system (3–5 kW_{el}). Therefore, the gasification unit has been designed considering a SOFCs stack able to provide 5 kW_{el}. The gasifier input power is between 11 and 12 kW_{th}, estimated considering a SOFCs stack efficiency of 45% and also taking into account the thermal losses through the gasification system. The test feedstock (wood pellets) has a lower heating value of 18–19 $MJ\ kg^{-1}$.

The characterization of the gasification process has been carried out considering the fuel gas required by the solid oxide fuel cells. Fuel gas for SOFCs has to be particle free, in order to avoid clogging of the gas channels, sulphur compounds free to avoid the poisoning of the cells and must have low tar content. In fact, the cells can tolerate a certain amount of tars because they can directly reform hydrocarbons which is also a way for the chemical cooling of the SOFC itself. This type of fuel cells, which work at high temperature, can accept different fuels in input, even if the standard fuels are hydrogen and methane.

Table 1
Syngas molar composition (dry basis) and char production, LHV and HHV and global process efficiencies.

(% molar fraction)	Partial oxidation ER = 0.20, T = 740 °C	Steam gasification SC = 0.50, T = 720 °C	Steam gasification SC = 3.00, T = 750 °C
H_2	29.35	51.93	62.80
CO	33.90	37.16	13.87
CO_2	5.23	8.36	23.26
CH_4	0.62	2.50	0.03
N_2	30.90	0.05	0.04
O_2	0.00	0.00	0.00
Char	0.00	0.00	0.00
LHV (MJ Nm^{-3})	7.57	11.05	8.43
HHV (MJ Nm^{-3})	8.16	12.16	9.65
Global process efficiency (%)	86.4	83.2	41.0

Syngas generated through biomass gasification shows higher hydrogen concentrations when pure steam or a mixture of air–steam is used as gasifying agent. Taking into account the need to maximize the hydrogen concentration in the syngas, the pure steam gasification process has been considered as the most suitable process for the purpose of this work.

The test gasifier is a downdraft fixed bed reactor with a cylindrical shape and it is externally heated by means of 4 electric ovens. The steam is provided by an internal coaxial tube (see Section 3.1). This particular configuration has been chosen to maximize the heat exchanges between the steam – fed at high temperature (up to 600 °C) – and the biomass bed in the reactor. The reactor geometry has been designed to ensure the nominal load capacity (2.5 kg h^{-1}) required to provide the 11–13 kW_{th} input load.

2.2. Thermodynamic approach

A thermodynamic analysis has been carried out by means of a 2-phase (gas–solid) thermodynamic model applied to the biomass conversion stage, based on the Cantera libraries [10]. The implemented solution algorithm is a version of the Villars–Cruise–Smith, based on the Gibbs energy minimization method. The model takes into account 60 different species for the gas phase, and 1 for the mass phase (i.e., graphite) [11]. The NASA [12] and Gri-Mech [13] databases have been used for the gas, water steam and char thermodynamic properties.

From the equilibrium analysis, and for the considered feedstock (i.e., spruce pellets), the optimum process efficiency has been obtained by means of partial oxidation. However, from a practical point of view, the steam gasification gives the highest syngas quality, since it is characterized by a higher concentration of hydrogen and it is not diluted by the atmospheric nitrogen as in the partial oxidation case; moreover, there is a lower production of char, due to a higher carbon conversion efficiency. On the other hand partial oxidation is a simpler conversion process as it has usually less practical heat transfer limitations for high temperature heat exchanges than steam gasification. The global process efficiency of both partial oxidation and steam gasification have been computed taking into account the feedstock and the syngas heating values, the reactions enthalpies and the enthalpies of the gasifying agents (1).

$$\eta = \frac{LHV_G \cdot \dot{m}_G - \Delta H_R - \Delta H_A \cdot \dot{m}_A - (\Delta H_W - \Delta H_{VAP} - \Delta H_S) \cdot \dot{m}_W}{LHV_B \cdot \dot{m}_B} \quad (1)$$

Tables 1 and 2 contain the results obtained for partial oxidation process with ER = 0.20, 740 °C conversion temperature and for steam gasification with SC = 0.5 and 720 °C conversion temperature. These values of the process parameters determine the operation conditions that lead to the optimum global efficiencies of the considered gasification process. Furthermore, it has also considered the steam gasification process with SC = 3 and 750 °C, that approaches to more realistic plant operation conditions.

2.3. FEM approach

The thermodynamic analysis of the designed steam gasification reactor has been extended on a 2-dimensional domain of the designed gasifier, coupling the heat and the momentum equations and solving the PDE's problem by means of a finite elements formulation.

The proposed model is based on a system of two PDE's, the heat conduction Eq. (2) and the Euler Eq. (3), defined in the stationary regime and in two dimensions. The flow field of the gasifier bed has been characterized by means of the Euler equation, since the viscous and volume forces have been considered negligible for the present analysis. For the purposes of the present analysis the bed material can be considered as a granular fluid and the resulting average value of its velocity is very low. The coupling of Eqs. (2) and (3) gives the temperature T and the velocity $\boldsymbol{u}$ (4) distributions as results.

$$(\lambda \nabla^2 T) = -\dot{Q}(T) \quad (2)$$

$$\rho(u \cdot \nabla)u = -\nabla p \quad (3)$$

$$\boldsymbol{u} = (u_y, u_z) = (v, w) \quad (4)$$

The PDE's discretization procedure has been performed with the finite element analysis by means of the Comsol Multiphysics® software [14]. The continuous computational domain (i.e., the biomass

Table 2
Enthalpy variation along the conversion process for several values of the gasifying agent inlet temperature.

	Enthalpy variation (kWh kg^{-1})		
	Partial oxidation ER = 0.20, T = 740 °C	Steam gasification SC = 0.50, T = 720 °C	Steam gasification SC = 3.00, T = 750 °C
$T_{gasifying}$ = 20 °C	0.58		
$T_{gasifying}$ = 100 °C	0.55	1.42	1.98
$T_{gasifying}$ = 200 °C	0.52	1.41	1.94
$T_{gasifying}$ = 300 °C	0.49	1.39	1.83
$T_{gasifying}$ = 400 °C	0.46	1.37	1.71
$T_{gasifying}$ = 500 °C	0.43	1.35	1.59
$T_{gasifying}$ = 600 °C	0.39	1.33	1.47

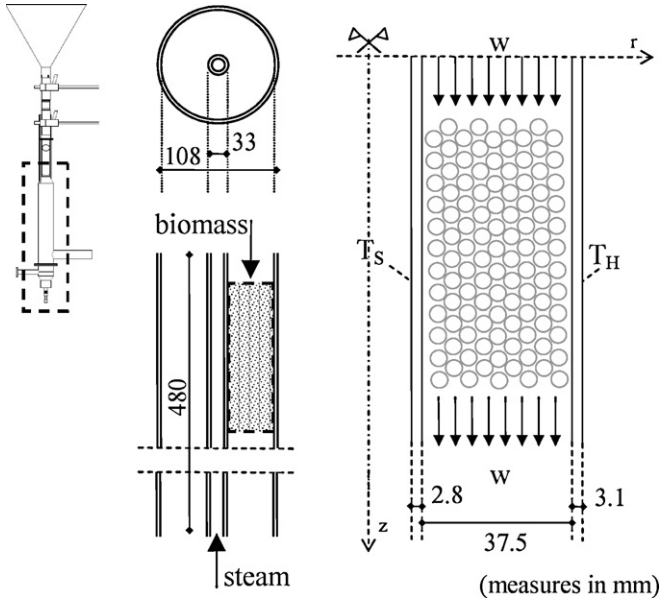

Fig. 1. 2D-axisymmetric reactor geometry.

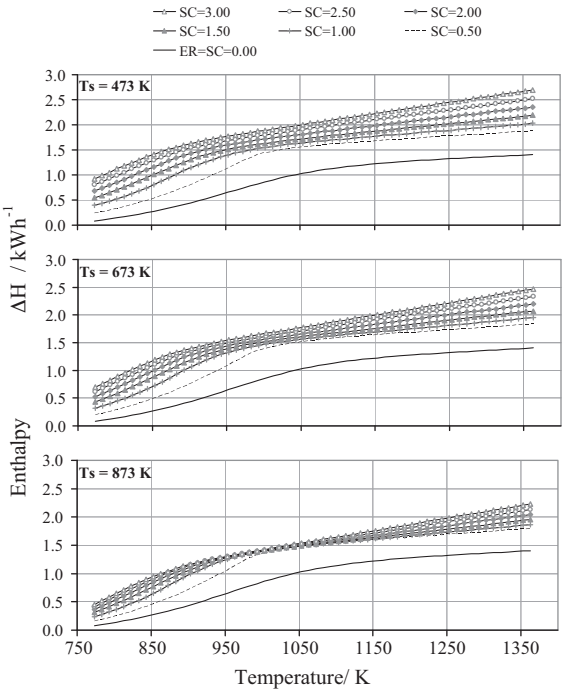

Fig. 2. Enthalpy variation along the process.

bed and the reactor walls) has been divided up into triangular elements, so that the unknown temperature field could be expressed by means of shape functions. These polynomial functions are completely defined inside each element by the temperature value in the nodal points. Thanks to the cylindrical shape of the reactor, the whole system has been discretized by a 2D-axisymmetric geometry (Fig. 1). The symmetry is characterized by a cross sectional plane, perpendicular to the upper and lower faces of the cylindrical reactor and delimited by the symmetry axis.

As boundary conditions for the heat conduction equation, temperature values have been assigned to the reactor external wall (T_E) and to the internal coaxial tube side (T_S) where the steam flows. Two adiabatic conditions have been assumed for the inlet (upper side) and outlet sections (lower side) of the reactor (5).

$$\boldsymbol{n} \cdot (\lambda \nabla T) = 0 \tag{5}$$

The steam temperature (T_S) has been estimated by means of an iterative algorithm. As a first guess, the steam temperature in the internal coaxial tube is set at the inlet value (temperature at the super-heater outlet). By means of several iterations, it is possible to compute the heat fluxes entering (or exiting) the steam tube, which are in equilibrium with the vertical temperature profile, which becomes the actual boundary condition.

The boundary conditions assumed for the Euler equation are represented by slip conditions on the reactor walls, assigned pressure (atmospheric value) at the reactor outlet and assigned velocity (i.e., average value on the cross section A) (6) at the reactor inlet

$$W = \frac{\dot{m}_B}{\rho_B \cdot A} \tag{6}$$

The model is structured by means of a three steps sequence. In the first step the source term of the heat equation is computed using a thermodynamic equilibrium routine as a function of the process parameters (temperature, pressure, steam to carbon ratio). Then the temperature and the velocity (plug flow regime) fields are evaluated with a finite element formulation in the second step; in this phase a 2D-axisymmetric representation of the reactor has been considered. The final computational step is the calculation of the reaction products profiles in the reactor in equilibrium with the computed temperature field. The characterization of the syngas is carried out estimating the local value of the concentration of the main gaseous compounds (H_2, CO, CH_4, CO_2, H_2O) and computing the average heating value. Moreover, the solid product residual fraction (char) – in equilibrium with the gaseous one – is also calculated.

The first computational step gives the heat equation source term as a function of the temperature, considering its dependence on the enthalpy variation along the conversion process, ΔH. The value of the enthalpy variation has been estimated using the aforementioned thermodynamic approach. The resulting curves (Fig. 2) – representing the enthalpy variations as a function of the temperature – have been parameterized for different values of SC ratio (i.e., the steam to carbon ratio) and of T_S (i.e., the steam temperature). The curves have been fitted with polynomial functions.

The representation of the source term (7) of the heat equation is based on the estimated polynomials and on the biomass flow rate that is subjected to the thermal treatment.

$$\dot{Q}(T) = -\Delta H(T) \cdot \frac{\dot{m}_B}{V} = -[H_{OUT}(T) - H_{IN}(T)] \cdot \frac{\dot{m}_B}{V} \tag{7}$$

The simulation has been carried out dividing the reactor in several elements ($i = 1, 2, \ldots, N$) along the vertical coordinate (z) and applying the FEM procedure to each subdomain step by step (Fig. 3). For the present simulations, the total number of subdomains has been assumed as $N = 10$ (i.e., $\Delta z = 48$ mm). The net available thermal power is calculated as the difference between the inlet (Q_{IN}) and outlet (Q_{OUT}) thermal power. The design value of the inlet thermal power has been assumed at 11–12 kW.

A correction factor (ξ) has been computed and applied to the heat source term (8), for each reactor subdomain next to the previous one (i.e., generic ith element). This factor (9) represents the biomass fraction converted along the gasification process down to the ith step.

$$\dot{Q}_{i+1}(T) = -\Delta H_i(T) \cdot \frac{\dot{m}_B}{V}(1 - \xi_i) \tag{8}$$

$$\xi_i = \sum_{k=1}^{i} \frac{(Q_{IN} - Q_{OUT})k}{(1/R)\int_0^R \Delta H_k(T, r)dr} \tag{9}$$

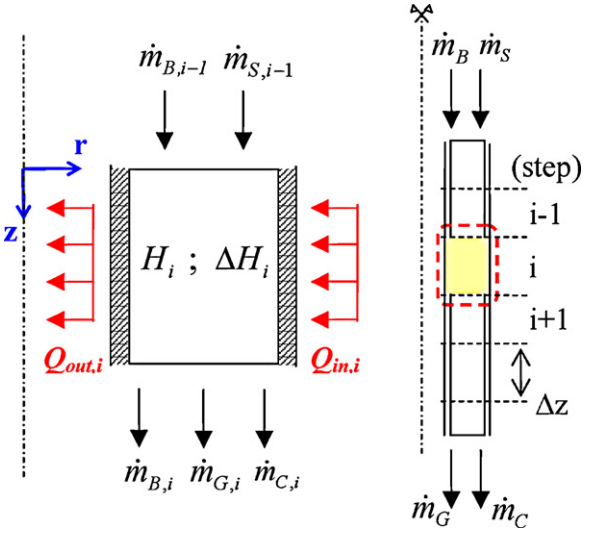

Fig. 3. Mass and energy balances.

The biomass fraction that is gasified depends on the ratio between the available thermal power (supplied to the system) and the energy required to sustain the gasification reactions (i.e., the enthalpy variation along the process). The former is computed as difference between the inlet and the outlet thermal flux, while the latter is computed as the average value on the reactor cross section.

Furthermore, considering that the initial mass of feedstock entering the system is continuously converted into syngas and char, the bulk physical properties of the biomass bed vary along the z-axis (10)–(13). The pellets porosity, whose average initial value ($\phi_{IN} = 0.49$) is deduced from the particle density (1150–1400 kg m^{-3}) and the bulk density (600–650 kg m^{-3}) of the material as stated by the producer, have been taken as reference parameters.

$$\phi_i = (1 + \xi) \cdot \phi_{IN} \tag{10}$$

$$\rho_{i+1} = \phi_i \cdot \rho_G + (1 - \phi_i) \cdot \rho_B \tag{11}$$

$$c_{p_{i+1}} = \phi_i \cdot c_{p_G} + (1 + \phi_i) \cdot c_{p_B} \tag{12}$$

$$\lambda_{i+1} = \phi_i \cdot \lambda_G + (1 - \phi_i) \cdot \lambda_B \tag{13}$$

The last step of the analysis is represented by the syngas characterization. For this purpose an estimation of the radial distribution of the main chemical compounds present in the gas phase and of the char production has been carried out. The results of the thermodynamic equilibrium computation are given as H_2, CO, CO_2, CH_4, H_2O concentrations and as char fraction produced, so that it is possible to compute the process conversion efficiency. For each computational step (i.e., subdomain), the temperature radial distribution obtained from the PDEs problem have been used to compute a local estimate (r, z) of the equilibrium products concentration in the reactor bed (Fig. 4).

3. Experimental procedures

The experimental apparatus designed and built is a CHP system based on a 5 kW$_{el}$ SOFC stack (SOFCpower) fueled with biomass syngas.

3.1. Gasification CHP unit

The steam gasification process is performed at atmospheric pressure in a 11 kW$_{th}$ (inlet power) co-current fixed bed gasifier, consisting of two coaxial cylindrical Inconel® vessels (1100 °C, 2 barg design), having external diameter of 102 mm, height of 480 mm, and net available volume of 0.0037 m^3. An internal coaxial tube of smaller diameter provides the gasifying agent (i.e., superheated steam). The gasifying unit is equipped with a steam generator (evaporator and super-heater) capable to supply steam up to 600 °C at 2 barg.

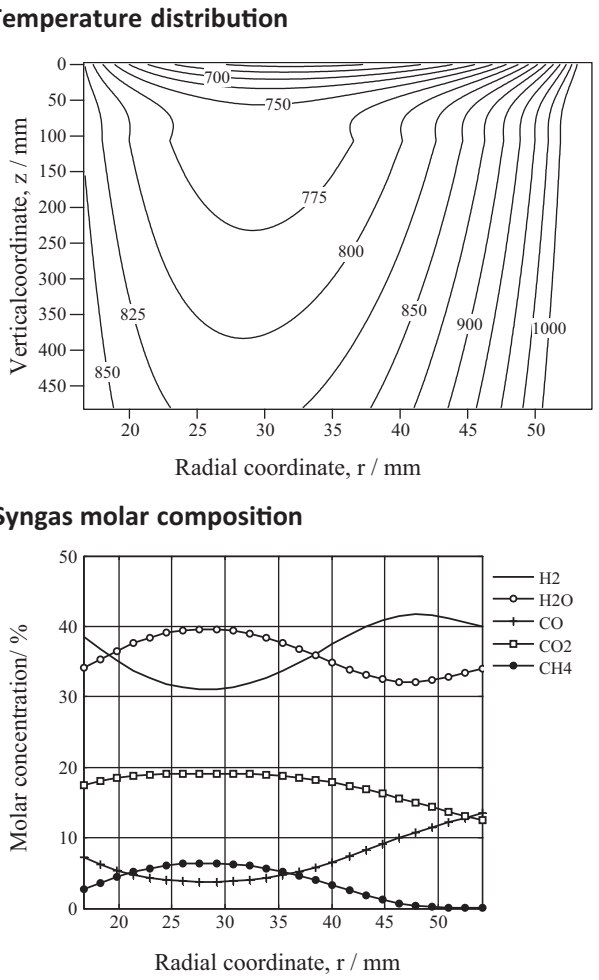

Fig. 4. Temperature distribution in the gasifier and local estimate of the equilibrium products concentration (z = 432 mm) in the reactor (SC = 2, T_H = 1073, T_S = 873).

The gasifier is externally heated by means of four ovens (maximum power 1 kW each). Temperature and pressure sensors are placed inside the reactor in order to control the process. A power meter measures the energy consumption of the ovens and of the steam generator during the heating phase and the gasification stage (stationary temperature stage). The biomass is stored in a closed hopper and fed in the reactor from the top, by means of an horizontal Archimedean screw. The feeding rate depends on the rpm (rounds per minute) of the screw which can be manually set by an inverter. The minimum feeding rate is 10 g min^{-1}.

A second Archimedean screw (of the same size) is placed at the bottom of the reactor to discharge the char produced during the gasification process. The starting and switching off of the screws is controlled via computer. The gasifier can work both in continuous and semi-continuous mode.

Wood pellets (spruce) have been used as feedstock for the experimental campaign (elemental analysis and heating value are reported in Table 3). The plant has been tested with pellets charge of 1, 1.5 and 2 kg h^{-1} (up to 80% of the nominal load which is 2.5 kg h^{-1}).

Table 3
Feedstock properties.

Ultimate analysis (% mass a.r.)				
C: 47.0	H: 6.1	O: 46.8	N: 0.01	S: <0.01
Moisture content (% mass a.r.)			7.0	
Ash (% mass a.r.)			0.2	
Lower heating value (MJ kg^{-1})			18.5	

The syngas is cooled and cleaned before performing the analysis by means of a portable Hp Agilent 3000 Micro GC able to measure the concentration of CO_2, O_2, N_2, CH_4, C_2H_2, C_2H_4, C_2H_6, H_2 and CO. The same GC has been used to detect the hydrogen sulphide concentration changing the gas carrier from Argon to Helium (Helium allows the measurements of CH_4, CO, CO_2, N_2 and H_2S).

The temperature field inside the reactor is characterized by means of three K-thermocouples placed at different height and radial positions. The PFD of the system is reported in Fig. 5.

3.2. Syngas characterization

The aim of the experimental activity is to produce a syngas suitable for solid oxide fuel cells, that implies high hydrogen content and low tar concentration. The experimental conditions to maximize the hydrogen concentration (temperature and SC) have been assessed by means of the equilibrium model described in Section 2.

Fifteen tests have been run during the experimental activity, as reported in Table 4. The gasification temperature investigated has been changed between 700 and 800 °C. The experimental activity has been divided in two phases: in the first one (tests from 1 to 7th) the influence of SC (changed between 2 and 3), reaction temperature and steam inlet temperature (from 200 °C to 600 °C) has been investigated. The reactor operated in a semi-continuous mode: the biomass has been fed, and the char discharged once every hour.

In the second phase (tests from 9 to 15th) the attention has been focused on the H_2S measurement with and without the presence of the catalyst. The gasification parameters, SC and steam temperature, have been kept constant at 2.5 and 600 °C respectively. The ovens temperature has been kept at 800 °C. In this way the experimental average temperature measured near the syngas outlet is about 750 °C. This value represents the average conversion temperature and it is in agreement with the conditions given by the equilibrium simulations to maximize the hydrogen concentration and the process efficiency (cf. Section 2.2). In this phase the gasifier operated in a continuous mode: the biomass and char have been continuously added and discharged, respectively. The feeding rate has been increased to 2 kg h^{-1}. Test no. 8 has been also run in order to measure the energy consumption of the empty system. Finally, two preliminary tests coupling the system with the SOFCs stack have been run (cf. Section 3.4).

By means of the known amount of nitrogen fed to the system through the feeding hopper, the syngas production has been estimated to be around 0.6–0.7 $Nm^3\ kg^{-1}_{pellets}$. The char produced during the steam gasification tests is approximately 18% of the initial biomass weight.

In Table 5 the average gas composition (N_2 free) has been reported for the 12 tests of which the gas composition has been analyzed. No remarkable differences can be observed in the first series of tests, in spite of the different SC values. The hydrogen concentration is higher than 60%, the methane production is very low and the carbon monoxide and carbon dioxide concentrations have been assessed at 5% and 30%, respectively. A change in the average gas composition has been observed in the second group of tests (9–12th) due to the different operation mode of the gasifier; indeed, because of continuous operation, the gas residence time inside the reactor is reduced and this implies lower H_2 and a higher CH_4 and CO concentrations (approx. 53%, 7% and 12%, respectively). Moreover, the gas heating value increases in the second group of tests due to higher concentration of fuel gases.

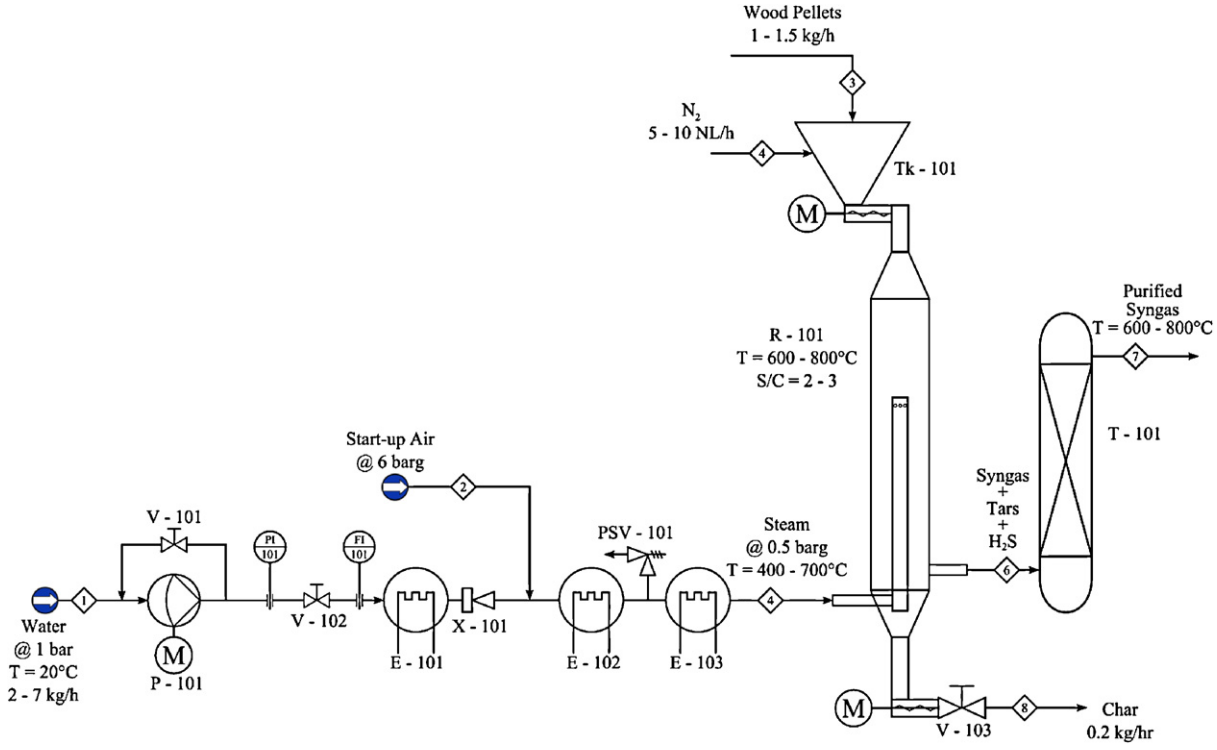

Fig. 5. PFD of the system.

Table 4
Tests performed during the experimental activity.

Test no.	T reactor	T steam	SC	Feeding	Catalyst	Gas analysis	Fuel cell
1	800 °C	200 °C	2	1 kg h^{-1}	–	H_2, CO, CO_2, CH_4, C_2H_2, C_2H_4, C_2H_6	–
2	800 °C	600 °C	2	1 kg h^{-1}	–	H_2, CO, CO_2, CH_4, C_2H_2, C_2H_4, C_2H_6	–
3	800 °C	400 °C	3	1.5 kg h^{-1}	–	H_2, CO, CO_2, CH_4, C_2H_2, C_2H_4, C_2H_6	–
4	800 °C	400 °C	2	1/1.5 kg h^{-1}	–	H_2, CO, CO_2, CH_4, C_2H_2, C_2H_4, C_2H_6	–
56	700 °C	400 °C	2	1.5 kg h^{-1}	–	H_2, CO, CO_2, CH_4, C_2H_2, C_2H_4, C_2H_6	–
6	700 °C	400 °C	3	1/1.5 kg h^{-1}	–	H_2, CO, CO_2, CH_4, C_2H_2, C_2H_4, C_2H_6	–
7	700 °C	400 °C	3	1/1.5 kg h^{-1}	–	H_2, CO, CO_2, CH_4, C_2H_2, C_2H_4, C_2H_6	–
8	800 °C	600 °C	2.5	–	–	–	–
9	800 °C	600 °C	2.5	2 kg h^{-1}	–	H_2, CO, CO_2, CH_4, C_2H_2, C_2H_4, C_2H_6	–
10	800 °C	600 °C	2.5	2 kg h^{-1}	–	H_2, CO, CO_2, CH_4, C_2H_2, C_2H_4, C_2H_6	–
11	800 °C	600 °C	2.5	2 kg h^{-1}	–	H_2S, CO, CO_2, CH_4, C_2H_2, C_2H_6	–
12	800 °C	600 °C	2.5	2 kg h^{-1}	Yes	H_2S, CO, CO_2, CH_4, C_2H_2, C_2H_6	–
13	800 °C	600 °C	2.5	2 kg h^{-1}	Yes	H_2S, CO, CO_2, CH_4, C_2H_2, C_2H_6	–
14	800 °C	600 °C	2.5	2 kg h^{-1}	Yes	–	Yes
15	800 °C	600 °C	2.5	2 kg h^{-1}	Yes	–	Yes

The height of the biomass bed is detected by means of the three thermocouples in the reactor. When the gasifier operates in semi-continuous mode, the biomass loads are clearly detected by the deepest and middle thermocouples. In fact, the temperatures registered by those sensors inside the biomass bed are around 100 °C, lower than the gasification temperature that is externally imposed. In the continuous mode, the biomass is loaded and discharged continuously and the height of the bed is detected by the middle thermocouple.

3.3. Catalytic filter

In order to directly feed a SOFC stack with the syngas obtained from gasification, a high temperature filtration system is required. This filter is required to have high cleaning efficiency at the operation temperature (700–800 °C) and possibility to be regenerated or easily disposed; moreover, considering that gasification is carried out at atmospheric pressure, the filter must have a low head loss.

The hot gas cleaning unit consists of a cylindrical vessel of 60.33 cm of diameter and 40 cm of length and it is placed downstream the gasifier. It is insulated and heated up to 815 °C by means of an electric oven. The aim of the catalyst is to reduce both the tar concentration, which decreases the fuel cell efficiency, and the hydrogen sulphide that is poisonous to the cells. A two stage filter was tested, consisting of a bed of calcinated dolomite used for tar cracking followed by a catalyst made of manganese oxide supported on zirconium silicate for hydrogen sulphide adsorption.

The efficiency of dolomite for tar cracking at high temperature (700–900 °C) has been investigated and proved by several authors [15–17]. On the contrary, for the hydrogen sulphide abetment, only catalysts guarantee up to a temperature of 450 °C are now commercially available. These catalysts are based on ZnO which, in a reducing environment, turns in metallic Zn that evaporates at 600 °C. For process temperatures between 600 and 1000 °C several catalysts are under investigation, but nothing is still available for industrial and commercial applications. Manganese oxide is a promising material for high temperature desulfurization for its good performances and low cost [18].

One of the main drawback in hot gas cleaning consists in the catalysts long regeneration time due to the low oxygen diffusion rate into the bulk of the sulphide catalyst. Some authors proposed to work with high space velocities and short adsorption time in order to use only the surface of the catalyst, letting the bulk unreacted [19]; this allows to obtain regeneration times similar to operation times but, on the other hand, leads to a inefficient utilization of the catalyst, being the bulk unused. A fine dispersion of sorbent material on a porous support may increase the catalyst adsorption capacity with respect to the sorbent mass and, at the same time, make possible a fast regeneration process.

The catalyst preparation follows the step described below:

1. Semi calcinated dolomite Semidol type K9/LB (Franz Mandt Gmbh) with a mean grain size of 2 mm has been calcinated at 1000 °C for 4 h.
2. Zirconium silicate supports have been produced by dipping polyester open cell sponge cylinders (d = 6 mm, L = 20 mm, pore density = 60 ppi, Eurotec) in a zirconium silicate slurry. The slurry was obtained by mixing zirconium silicate powder with Darvan C-N (RT Vanderbilt) and distilled water with a weight ratio of 40/1/10, in Turbula for 6 h. After mixing, 1 g of Duramax B-1000 binder (Rohm and Haas) was added for 15.3 g of suspension.
3. The supports have then been dried in oven at 80 °C overnight and then calcinated according to the following programme: RT to 300 °C in 5 h, 300 °C to 1350 °C in 5 h 50 min, dwell at 1350 °C for 3 h, free cooling.

Table 5
Average gas composition of the tests performed.

Test no.	Char (g kg^{-1})	C_2H_2 (% vol)	C_2H_4 (% vol)	C_2H_6 (% vol)	CH_4 (% vol)	CO (% vol)	CO_2 (% vol)	H_2 (% vol)	H_2S (ppm)	LHV (MJ Nm^{-3})
1	n.a.	0	0.00	0.00	1.3	4.2	29.2	63.4	–	7.85
2	175	0	0.00	0.00	1.5	7.0	28.2	63.1	–	8.22
3	150	0	0.00	0.00	1.4	3.7	30.0	64.9	–	7.96
4	n.a.	0	0.01	0.01	1.9	6.6	27.2	64.3	–	8.46
5	177	0	0.03	0.03	2.9	3.6	30.4	63.0	–	8.35
6	180	0	0.03	0.03	2.9	3.6	30.4	63.0	–	8.32
7	200	0	0.03	0.03	3.5	4.0	28.4	64.0	–	8.71
8	–	–	–	–	–	–	–	–	–	
9	172	0	0.91	0.40	6.46	11.8	29.1	51.2	–	10.13
10	182	0	0.85	0.37	6.24	12.3	28.15	52.1	–	10.15
11	177	–	–	–	6.37	9.8	25.7	53.72	84	9.3
12	n.a.	0.1	–	0.6	6.2	13	25.7	52.0	15	9.9
13	180	0.1	–	0.44	7.47	9.9	29.2	52.8	25	9.9

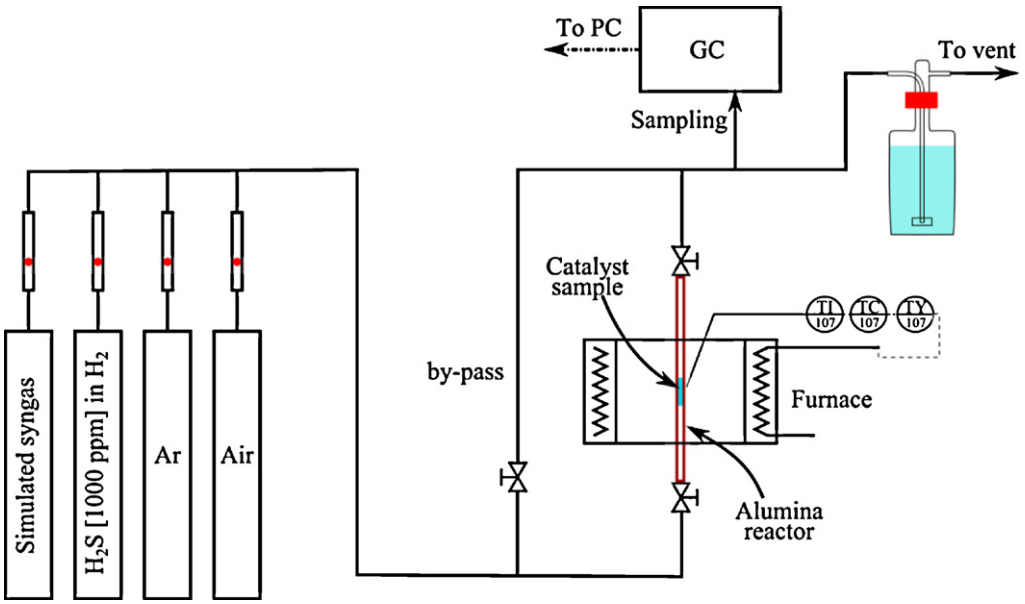

Fig. 6. Lab apparatus for testing the catalyst.

4. 20 g of supports have been introduced in a jar containing 100 mL of a 0.5 M solution of Manganese nitrate tetrahydrate (Sigma–Aldrich) and gently stirred for 1 h; after drying in oven at 80 °C for 6 h, the supports were finally calcinated at 850 °C for 2 h.

Before adding the catalyst to the gasifier filter unit, it has been tested in a alumina tubular reactor heated in a furnace (Fig. 6). The reactor can be fed with different gases. Two tests have been carried out: in the first 0.5 g of fresh catalyst kept at 600 °C has been fed with 1000 ppm of H_2S in H_2; in a subsequent test the same amount of fresh catalyst has been tested with a simulated syngas composed by 234 ppm of H_2S, 3% of CH_4, 20% CO, 12% CO_2, 20% H_2 and 45% of N_2. The hydrogen sulphide concentration downstream the catalyst is measured by means of a portable Hp Agilent 3000 Micro GC.

The catalyst has shown good performances when fed with hydrogen containing 1000 ppm of H_2S, being the concentration of H_2S at the outlet lower than 10 ppm for 40 min. The inlet flow rate varied from 40 to 200 NmL min^{-1} so that the amount of sulphur adsorbed is 5.8 $mg_S\ g_{cat}^{-1}$ (Fig. 7a).

In the experiment with the simulated syngas containing an inlet concentration of 234 ppm of H_2S, the catalyst has adsorbed H_2S for almost 2 h. Considering a gas flow of 107.4 NmL min^{-1}, the amount of sulphur adsorbed is 8.6 $mg_S\ g_{cat}^{-1}$ (Fig. 7b).

The H_2S concentration in the syngas produced by the steam gasifier is around 85 ppm (test no. 11). The gasification test nos. 12 and 13 have been run with the presence of the catalyst. The catalytic filter has been filled with a mixture of calcined dolomite (300 g) and 300 g of silica support impregnated with manganese oxides.

The results are reported in Table 5. The catalyst has shown positive performances, however the gas cleaning session could be improved to guarantee higher syngas quality.

3.4. SOFC performance

Finally, the gasifier has been coupled with a SOFC stack and some preliminary tests have been performed. Even if the gasifier has been designed to be coupled with a 5 kW fuel cells stack, the preliminary tests have been run with smaller stacks of 250 W (test no. 14) and 330 W (test no. 15) to verify the feasibility of the coupling between the gasifier and the SOFCs stack.

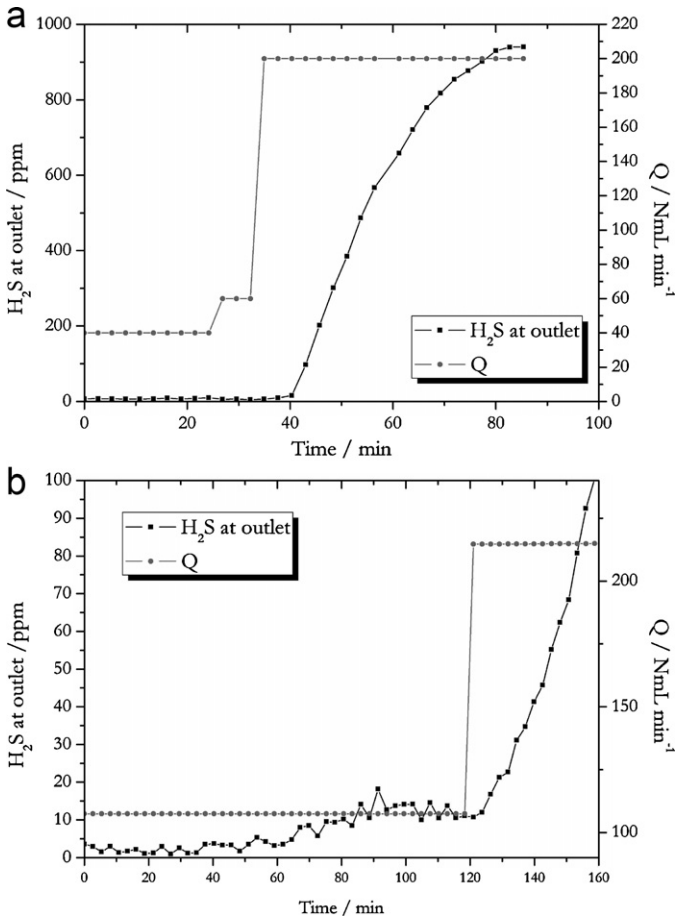

Fig. 7. H_2S abetment considering a mixture of H_2 and H_2S concentration of 1000 ppm in (a) and a simulated syngas with 234 ppm of H_2S in (b).

The stacks are designed to have an electric efficiency of 45% (on the fuel LHV) at 70% of the fuel utilization. These fuel cell stacks achieves a specific power density of 0.3 W cm^{-2} of active area at a cell potential of 0.7 V and a current density of 0.428 A cm^{-2}. The active area of each cell is 50 cm^2. Considering the characteristics

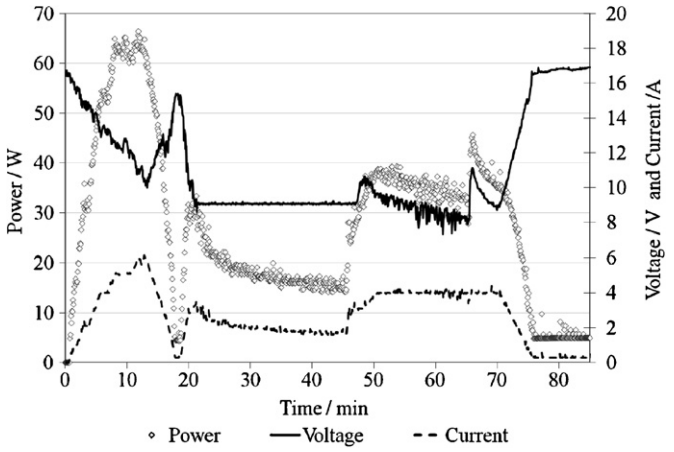

Fig. 8. Voltage, current and power density of the test no. 14 (power stack: 250 W).

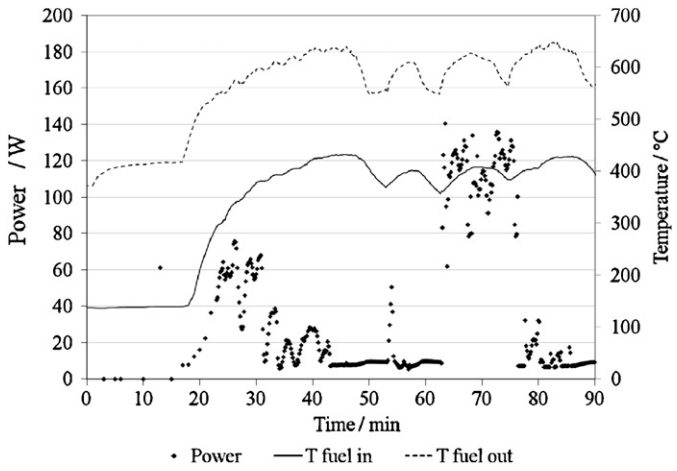

Fig. 9. Power produced and inlet and outlet fuel temperature of test no. 15 (power stack: 330 W).

of the cells, 3 clusters of 6 cells each are needed to reach 250 W, and 4 clusters for 330 W. Considering the enthalpy of the reactions (14)–(16) and the moles of H_2, CO and CH_4 in the inlet syngas, the whole reaction enthalpy is −11,755 kJ per hour, corresponding to an input power of 3.26 kW.

$$H_2 + 1/2O_2 \rightarrow H_2O \quad (14)$$

$$CO + 1/2O_2 \rightarrow CO_2 \quad (15)$$

$$CH_4 + 2O_2 \rightarrow 2H_2O + CO_2 \quad (16)$$

The number of oxygen moles required for 100% fuel utilization in the fuel cell is calculated with (17).

$$\text{Mol of } O_2 = 0.5\,(\text{mol of } H_2) + 0.5\,(\text{mol of CO}) + 2\,(\text{mol of } CH_4) \quad (17)$$

Considering the average syngas composition and production measured during the experimental activity, the yields in mol per hour are: H_2 = 31.6 mol h^{-1}; CO = 7.42 mol h^{-1}; CH_4 = 3.9 mol h^{-1}; CO_2 = 17.3 mol h^{-1}, for a feeding rate of 2 kg h^{-1}. By means of (17) the moles of oxygen needed for the full fuel utilization have been computed as 27.34 mol h^{-1}. Thus, the flow rate is 0.66 Nm^3 h^{-1} of oxygen, or 3.2 Nm^3 h^{-1} of air.

Since the fuel cell stacks tested are undersized with respect to the available syngas, only 15–20% of the produced syngas is fed in the stack. All the syngas generated at the tested feeding rate (2 kg h^{-1}) can supply a 2.5 kW SOFC stack, considering a fuel utilization of 70%.

In Fig. 8 the voltage, current and power of the fuel cell stack measured during the test 14 are reported. The stack has worked for approximately 80 min before stopping due to the poisoning of the cells. There has been a peak of power production of 65 W, after a period of increasing and decreasing of the power. Before the switching off, an almost stable period of operation has been registered for 20 min with a power production of 30–35 W. Since the nominal power is 250 W (using pure hydrogen as fuel), the stack has worked at 18% of its nominal power (considering the performance of the more reliable stable period). During the initial peak of production, the stack has worked at 24% of its nominal power, even if for a short time.

In the last test (no. 15) a stack of 24 cells has been coupled with the gasifier (4 clusters) for a nominal power of 330 W.

Fig. 9 shows the power generated by the SOFC stack and the fuel input and output temperatures. In the first phase, 60 W have been generated for approximately 10 min, then the stack performance has rapidly decreased. The feeding of the syngas has been stopped for 10 min to clean the SOFCs with the so called "forming gas" (nitrogen with 5% of hydrogen). In the second part of this test, 130 W have been produced for 15 min, then the SOFCs performance has decreased again and the test has been stopped. The cell efficiency has been assessed at 18% during the first phase (60 W produced) and at 40% during the second phase (130–140 W produced).

It is worth to highlight that the tested fuel cells are themselves prototypes of a local industry, and some problems related to the non-correct operation of the SOFCs can occur during the gasification tests.

4. Results and discussion

4.1. Energy and carbon balance

The energy and carbon balance have been assessed on the basis of all the performed tests.

The carbon balance has been assessed using the biomass mass flow rate and elemental composition as inputs and the products (syngas and char) composition and specific production per kg of biomass as outputs. From the char elemental composition, reported in Table 6, it has also been possible to calculate the char heating value. Moreover, in order to compute the carbon balance a value of 60 mg Nm^{-3} for tar production has been considered [20].

The energy balance has been also estimated considering the input and output energy fluxes measured by means of the biomass, syngas and char characteristics and thanks to some energy meters installed on the experimental plant. Those devices measure the electric consumption of both the steam generator and the reactor.

The carbon balance has been closed, for all the tests, with an error of ±8%. The system overall energy efficiency has been assessed around 40%. This value is in agreement with the efficiency calculated by means of the thermodynamic model described above (Table 1). The energy required by the electric ovens and by the steam generator has been compared with the theoretical calculations obtained by means of the thermodynamic model. The comparison between the predicted and measured

Table 6
Char properties.

Char ultimate analysis (% mass a.r.)				
C: 91.35	H:1.75	O:6.73	N:0.17	S < 0.01
Moisture content (% mass a.r.)			1.8%	
Ash (% mass a.r.)			1.5%	
Lower heating Value (MJ kg^{-1})			28.7	

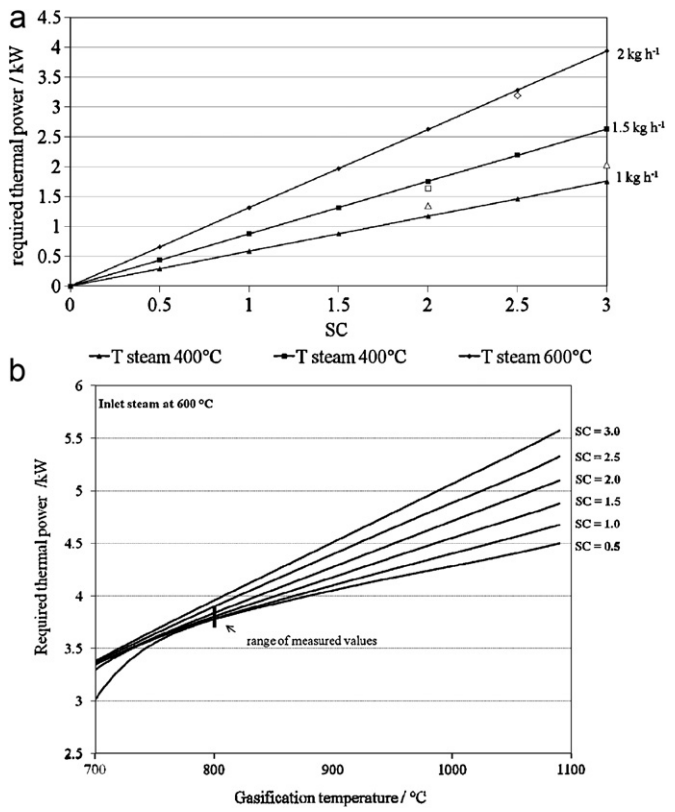

Fig. 10. Comparison between calculated (lines) and measured (points) energy data of (a) the steam generator at different steam temperature and feeding rate (b) the reactor at different SC and steam temperature of 600 °C.

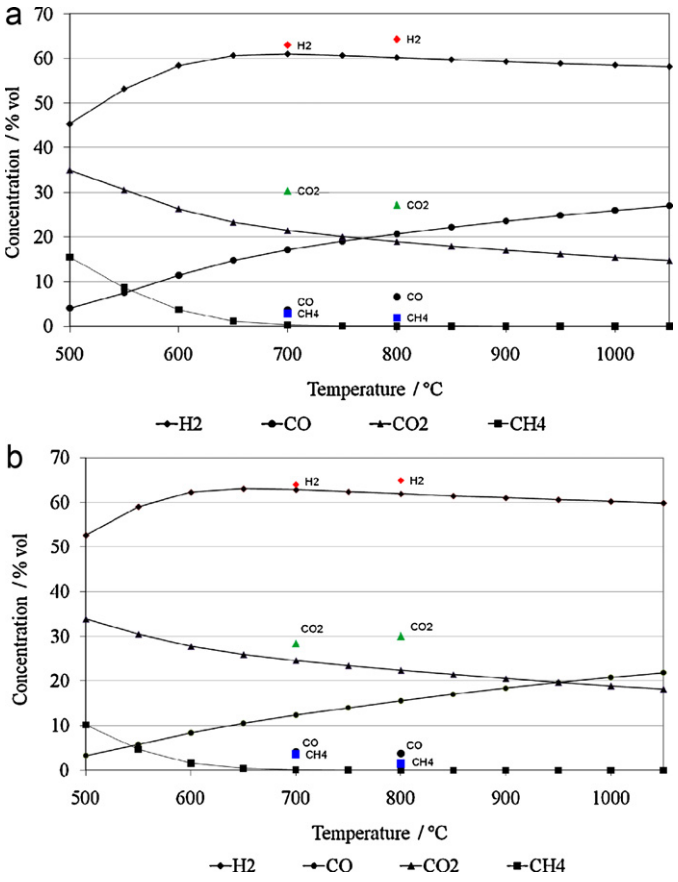

Fig. 11. Syngas composition foreseen by the equilibrium model for SC = 2 (a) and SC = 3 (b) versus experimental average gas composition (points).

data is reported in Fig. 10 and a good agreement can be clearly observed.

5. Model calibration

The syngas composition and LHV predicted by the equilibrium model for the steam gasification process (SC = 2, SC = 3) versus the average gas composition measured is reported in Figs. 11 and 12. For the first group of tests the model shows a good agreement for the H_2 prediction, an overestimation of the CO and underestimation of CO_2. Anyway, the lower heating values predicted by the model are in good agreement with the values calculated considering the average syngas composition for the first series of test. For the second group, the higher methane concentration (not predicted by the model) increases the syngas heating value.

As shown by previous literature studies, a correct methane estimation by means of a thermodynamic model is a difficult task, since it is not an equilibrium compound [21–23]. The high concentrations of methane – measured in a real reactor – can result from incomplete conversion of pyrolysis products (tars) and thus cannot be explained on a purely thermodynamic basis.

In the first seven tests the modeling results are in good agreement, since the methane production is very low due to the reactor configuration that allows a high residence time. In the second series of tests, the methane production is significantly higher with values around 7%.

However, the gas heating value predicted by the model is in good agreement with the experimental values.

As a whole, many authors have proposed different approaches in order to achieve a better agreement between equilibrium model predictions and experimental data. A possible approach is the application of empirical parameters in order to modify the carbon conversion or to correct directly the methane fraction in the syngas [21,22,24].

The high percentage of the residual fraction formed during the gasification process contains approximately 40% of the initial moles of carbon. These moles, which remain in solid phase, do not participate in carbon monoxide, methane and carbon dioxide formation. The model has been calibrated according to the experimental data to take into account the residual solid phase and the methane production. The carbon conversion efficiency (i.e., the ratio between

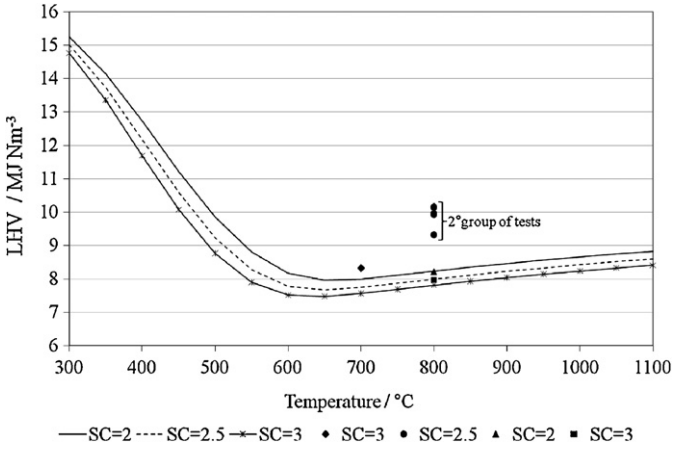

Fig. 12. Syngas composition foreseen by the equilibrium model for SC = 2 (a) and SC = 3 (b) versus experimental average gas composition (points).

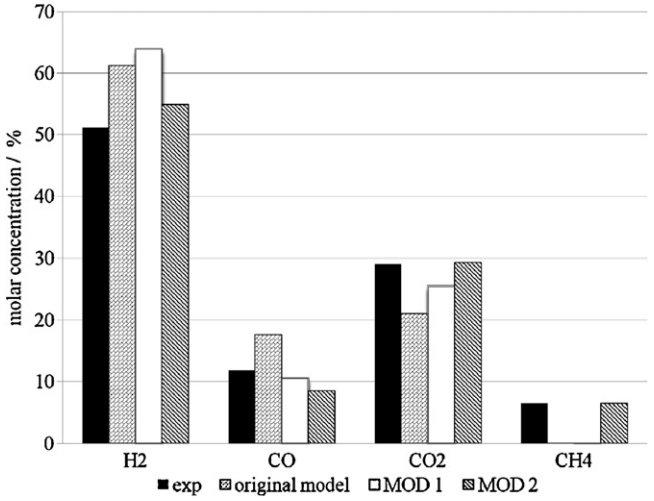

Fig. 13. Comparison between the experimental data (exp) and the original and modified model for test no. 9. MOD1 is the model modified with the η_c parameter, and the MOD2 includes also the n_1, n_2 parameters.

the number of carbon moles converted in gas and the total carbon moles fed) has been calculated with (18).

$$\eta_c = \frac{c_{gas}}{c_{fed}} \tag{18}$$

Then the initial input vector of the model, which contains the number of moles of C, H, O, N, S per kg of biomass fed, has been modified according to the η_c value (19).

$$N^0_{input} = [n_C, n_H, n_O] \Rightarrow N^1_{input} = [\eta_c n_C, n_H, n_O] \tag{19}$$

To take into account also the methane formation, the experimental gas composition has been used to evaluate the moles of carbon (n_1) and hydrogen (n_2) converted into methane during the process. The initial composition is corrected considering the η_c and subtracting the moles of carbon and hydrogen arising from the previous calculation (20).

$$N^1_{input} = [\eta_c n_C, n_H, n_O] \Rightarrow N^*_{input} = [\eta_c n_C - n_1, n_H - n_2, n_O] \tag{20}$$

In Fig. 13 the experimental gas composition of test no. 9 has been compared with the original and the modified models outputs.

The agreement between experimental and modeling data, considering only the carbon conversion parameter (output of MOD1), has been remarkably improved. However, in order to achieve a better agreement, is worth to also calibrate the methane concentration in the syngas, as clearly shown by the output of MOD2. The range of temperature and SC investigated in the present experimental activity is not wide enough to find out experimental correlations capable to estimate the methane and carbon conversion. However, as found by other authors through extensive experimental campaigns, it is possible to find out experimental correlation between the gasification parameters and carbon conversion, i.e., between the carbon conversion and the ER value [18]. From one side the use of empirical correlations limits the predictive capability of a thermodynamic model to specific process conditions (i.e., reactor type and design). However, from the other side, the resulting 'quasi-equilibrium' model becomes an useful tool to assess the gas composition and yield with satisfying accuracy for configurations similar to the test case.

To test the reliability of the 2D FEM model described in Section 2.3, the temperature data measured by the thermocouples placed inside the reactor, at different radial positions and heights, have been compared with the temperature profiles simulated by

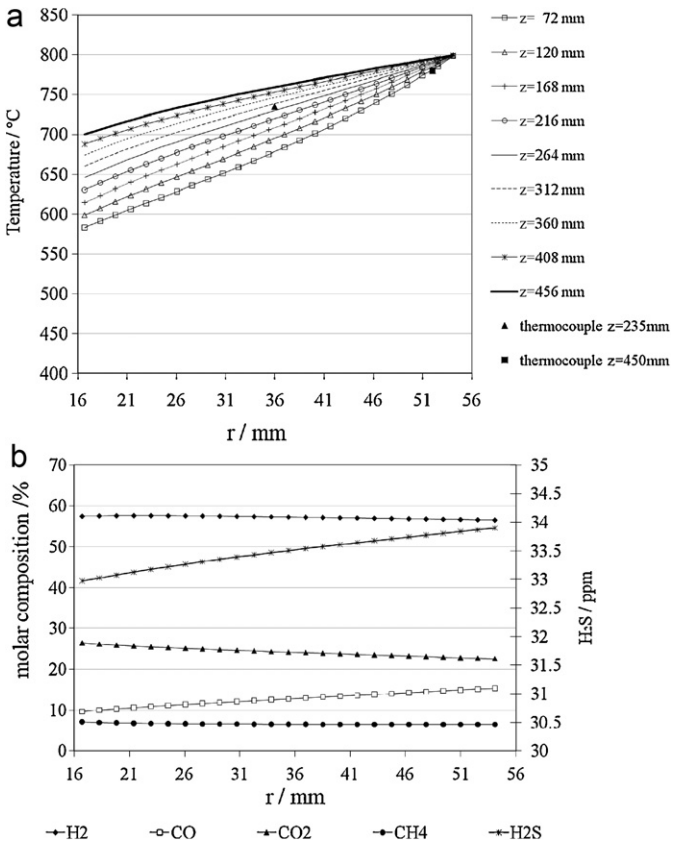

Fig. 14. (a) Reactor temperature simulated by the finite element model; (b) syngas composition simulated by the modified equilibrium model for $z = 456$ mm.

the model. The experimental temperatures range between 700 and 800 °C, while the computed ones are between 500 and 600 °C.

The finite element model takes into account only the heat transfer through conduction. The deviations between the experimental data and the model outputs, have confirmed the influence of the heat exchanges through radiation and convection. In order to calibrate the model response, a single heat transfer coefficient (i.e., thermal transmittance) has been estimated using the experimental data. The estimated thermal transmittance has been defined as an "apparent thermal conductivity" including the contribution of the convection and radiation. For this purpose, the Fourier equation for heat conduction (21) in one-dimensional case, using non-dimensional parameter (22) has been considered.

$$\frac{\partial^2 \Theta}{\partial \gamma^2} + 2\gamma \frac{\partial \Theta}{\partial \gamma} = 0 \tag{21}$$

$$\Theta = \frac{T - T_i}{T_O - T_i}; \quad \gamma = \frac{x}{2\sqrt{a\tau}} \tag{22}$$

A time dependent boundary condition has been applied, in agreement with the heating rate of the oven. The solution of heat equation in a semi-infinite solid body has been assumed for the purpose of the present analysis. The solution is represented by the error function (*erf*).

$$\Theta = \frac{T_f - T_i}{T_O - T_i} = 1 - \frac{2}{\sqrt{\pi}} \int_0^{\gamma} e^{-z^2} dz = 1 - erf(\gamma) \tag{23}$$

The solution of the integral of the *erf* function is not known in an explicit form. The values of the error function are tabled [25]. Thanks to the temperature measurements, it has been possible to obtain the heating time for the biomass starting from the initial T_i to the final temperature T_f. Thus, the Θ and the γ values have been

calculated. From the definition of γ it is possible to deduce λ, the apparent thermal conductivity of the solid body (24).

$$\lambda = \left(\frac{x}{2y}\right)^2 \cdot \frac{\rho c_p}{\tau} \quad (24)$$

The apparent thermal conductivity adopted in the finite element model is an average of the λ values calculated by means of the experimental data of the experimental tests. The estimated thermal conductivity is $1.23\,W\,m^{-1}\,K^{-1}$.

The 2D model – corrected with the apparent thermal conductivity – has been coupled with the quasi-equilibrium model, to take into account the biomass conversion in char and methane. The temperature profiles are shown in Fig. 14. One of the thermocouples is located at 235 mm from the top of the reactor and equidistant from the reactor wall and the central coaxial tube. The data measured by the sensor show a good agreement with the simulated temperature. The predicted temperature profiles inside the reactor can be reasonably considered close to the real one.

6. Conclusions

At present, the biomass thermochemical conversion processes and their applications for heat and power generation are object of several research studies, to find out efficient systems to exploit the energy content of biomass.

The present work aims to improve the knowledge on the potential of the steam gasification process for power generation in small scale applications. The syngas produced via steam gasification process seems to be a suitable fuel both for internal combustion engines and for solid oxide fuel cells due to its high hydrogen content.

Engineering models are usually applied to design and evaluate the performances of gasification systems. A thermodynamic equilibrium model has been used to estimate the syngas composition. The positive aspect of the thermodynamic approach lays in its applicability to several systems without a deep knowledge of the reaction mechanisms. Thus, it can be successfully applied to determine the maximum theoretical performance of a biomass conversion process.

A continuous small scale steam gasification system has been set up and tested. The syngas produced has a hydrogen content ranging between 50 and 60% and a LHV of $8\,MJ\,Nm^{-3}$. Considering its composition and energy content, the obtained syngas is a suitable fuel for fuel cells. However, the gas cleaning is still one of the main critical issues. In particular the tar and the H_2S in the gas can rapidly decrease the life of the fuel cells. The tested catalyst shows a satisfying efficiency in H_2S and tars abatement even if for a short period of operation, after which the stack performances decrease. This fact may be attributed to filter undersize.

A satisfactory agreement has been found between the experimental data and the modeling simulations calibrated by means of the data collected during the experimental activity. A good agreement has been also observed between the calculated and measured energy fluxes required by the system in order to sustain the conversion process.

The thermodynamic approach has been confirmed to be a simple engineering tool useful to assess with good reliability the theoretical performance of a gasification system, knowing only the main gasification parameters.

Acknowledgments

The authors are grateful to the Provincia Autonoma di Trento that has funded this project and to Eurocating S.p.a. that has led its development. The authors would like to thank also SOFCpower S.p.a for providing the SOFC stacks. The authors are grateful to Damiano Avi of the Department of Physics of the University of Trento for the GC analyses.

References

[1] V. Alderucci, P. Antonucci, G. Maggio, N. Giordano, V. Antonucci, Int. J. Hydrogen Energy 19 (1994) 369–376.
[2] K.D. Panopoulos, L.E. Fryda, J. Karl, S. Poulou, E. Kakaras, J. Power Sources 159 (2006) 570–585.
[3] K. Panopoulos, L. Fryda, J. Karl, S. Poulou, E. Kakaras, J. Power Sources 159 (2006) 586–594.
[4] S. Cordiner, M. Feola, V. Mulone, F. Romanelli, Appl. Therm. Eng. 27 (2007) 738–747.
[5] A.O. Omosun, A. Bauen, N.P. Brandon, C.S. Adjiman, D. Hart, J. Power Sources 131 (2004) 96–106.
[6] M. Liu, P.V. Aravind, T. Woudstra, V.R.M. Cobas, A.H.M. Verkooijen, J. Power Sources (2011), doi:10.1016/j.jpowsour.2011.02.065.
[7] F.P. Nagel, J.T. Schildhauer, S.M. Biollaz, Int. J. Hydrogen Energy 34 (2009) 6809–6825.
[8] F.P. Nagel, J.T. Schildhauer, N. McCaughey, S.M. Biollaz, Int. J. Hydrogen Energy 34 (2009) 6826–6844.
[9] F.P. Nagel, S. Ghosh, C. Pitta, T.J. Schildhauer, S. Biollaz, Biomass Bioenergy 35 (2011) 354–368.
[10] D. Goodwin, Cantera: object oriented software for reacting flows, California Institute for Technology (Caltech), 2006, http://www.cantera.org (accessed January 2011).
[11] M. Baratieri, P. Baggio, L. Fiori, M. Grigiante, Bioresour. Technol. 99 (2008) 7063–7073.
[12] B.J. McBride, S. Gordon, M.A. Reno, NASA Report TM-4513, 1993.
[13] G.P. Smith, D.M. Golden, M. Frenklach, N.W. Moriarty, B. Eiteneer, M. Goldenberg, C.T. Bowman, R.K. Hanson, S. Song, W.C. Gardiner Jr., V.V. Lissianski, Z. Qin, GRI-Mech 3.0, 2007, http://www.me.berkeley.edu/gri_mech (accessed July 2007).
[14] Comsol Multiphysics 3.3, http://www. comsol.com, 2008.
[15] A. Olivares, M.P. Aznar, M.A. Caballero, J. Gil, E. Frances, J. Corella, Ind. Eng. Chem. Res. 36 (1997) 5220–5226.
[16] A. Orio, J. Corella, I. Narvaez, Ind. Eng. Chem. Res. 36 (1997) 3800–3808.
[17] P. Perez, P.M. Aznar, M.A. Caballero, J. Gil, J.A. Martin, J. Corella, Energy Fuel 11 (1997) 1194–1203.
[18] A.T. Atimtay, L.D. Gasper-Galvin, J.A. Poston, Environ. Sci. Technol. 27 (1993) 1295–1303.
[19] M. Flytzani-Stephanopoulos, M. Sakbodin, Z. Wang, Science 312 (2006) 1508–1510.
[20] K. Umeki, K. Yamamoto, T. Namioka, K. Yoshikawa, Appl. Energy 87 (2010) 791–798.
[21] L. Liinanki, N. Lindman, S.-O. Sjöberg, E. Ström, in: R.P. Overend, T.A. Milne, L.K. Mudge (Eds.), Fundamentals of Thermochemical Biomass Conversion, 1982 Esters Park, Colo, Elsevier Applied Science Publishers Ltd, England, 1985, pp. 923–936.
[22] M.J. Prins, K.J. Ptasinski, F. Janssen, Energy 32 (2007) 1248–1259.
[23] X. Li, Fuel 80 (2001) 195–207.
[24] M. Baratieri, E. Pieratti, T. Nordgreen, M. Grigiante, Waste Biomass Valoriz. 1 (2010) 283–291.
[25] F.P. Incropera, D. Dewitt, Fundamentals of Heat and Mass Transfer, Wiley and Sons Ltd, 2006.